

Sensitivity of quantum information to environment perturbations measured with the out-of-time-order correlation function

Mohamad Niknam,^{1,2,*} Lea F. Santos,³ and David G. Cory^{1,4,5,6}

¹*Institute for Quantum Computing, University of Waterloo, Waterloo, ON, Canada, N2L3G1*

²*Department of Physics, University of Waterloo, Waterloo, ON, Canada, N2L3G1*

³*Department of Physics, Yeshiva University, New York, New York 10016, USA*

⁴*Department of Chemistry, University of Waterloo, Waterloo, ON, Canada, N2L3G1*

⁵*Perimeter Institute, University of Waterloo, Waterloo, Canada, N2L2Y5*

⁶*Canadian Institute for Advanced Research, Toronto, ON, Canada, M5G1Z8*

(Dated: August 15, 2018)

Measures to quantify the flow of quantum information and its sensitivity to environment perturbations are needed to better understand the evolution of open quantum systems and to distinguish non-Markovian from Markovian dynamics. Here, we show that the extent of correlations in many-body quantum systems is an experimentally accessible metric for quantifying the spread of quantum information. Our experiment applies multiple-quantum nuclear magnetic resonance (NMR) technique to take snapshots of the multi-spin correlations between a central spin and the spins in its surrounding environment. We argue that the width of the distribution of these multi-spin correlations is the natural metric for quantifying the flow of information between the system and the environment. Quantum information shared between the two is sensitive to environment perturbations. The out-of-time-order correlation function (OTOC) is used to measure this sensitivity. By analyzing the decay of the OTOC as a function of our metric instead of time, we demonstrate the exponential behavior of the OTOC.

Non-Markovian system-environment dynamics remains one of the most challenging barriers to implementing quantum information processing. Such processes cause not only loss of information [1, 2], as it happens also with Markovian environments, but they allow information to flow back to the system qubit, resulting in interference and corruption of quantum information [3, 4]. Various tests have been proposed to quantify non-Markovianity, including the backflow of quantum Fisher information (QFI) [5, 6]. The QFI associates the information content of a quantum system with the precision of an unbiased parameter estimation, the Cramér-Rao bound [7]. When quantum information from the system qubit is shared with the environment, the QFI in the environment increases. Here, we analyze the dynamics of this shared quantum information in the central spin model by experimentally measuring the number of correlated spins between the system and the environment. We discuss the connection between this quantity and the QFI.

The study of the quantum evolution of spin systems in contact with an environment has had a pivotal role in our understanding of the problem of quantum information loss [8–10]. The central spin model, which in its simplest form consists of a single spin-1/2 interacting with environment spins that may also be coupled, provides a versatile platform for such studies [11–14]. Solid state nuclear magnetic resonance (NMR) is particularly suitable for the investigation of the central spin model, because techniques are available to separate the system-environment evolution from the internal evolution of the environment spins [15–17]. This allows us to examine the impact of each process individually.

The evolution under the system-environment Hamiltonian

leads to the growth of correlations between the central spin and the environment spins. Quantum information shared by the two is encoded in the form multi-spin correlations. We design an echo experiment capable of measuring the extent of these correlations and relate the number of correlated spins with the QFI.

In Markovian environments, the system-environment multi-spin correlations either do not exist or are short-lived. The life-time of these correlations is therefore associated with the level of non-Markovianity of the environment. In the absence of internal interactions in the environment, these correlations are long lived and the initial uncorrelated state of the system can be refocused with spin echoes. However, the dynamics in the environment can swap the states of the spins and scramble quantum information which results in the decline of the echo signal.

To quantify the sensitivity of the quantum information shared by the system and the environment, we analyze how the multi-spin correlations are affected by the environment dynamics. For this, we measure the out-of-time-order correlation function (OTOC),

$$F(T) = \langle W^\dagger(T)V(0)^\dagger W(T)V(0) \rangle, \quad (1)$$

where V and W are two unitary operators that commute or their commutator is small at time $T = 0$. To measure the OTOC, one needs to reverse the time evolution of $W(T)$, which makes NMR echo experiments the method of choice. The evolution of the OTOC was previously studied with ion traps [18, 19] and nuclear spins [20, 21].

The OTOC, often written as $\mathcal{C}(T) = -\langle [W(T), V(0)]^2 \rangle = 2\text{Re}[F(T)] - 2$, has become a central quantity in the analysis of the scrambling of quantum information in black holes and quantum systems. For Hamiltonians with short-range interactions, Lieb and Robinson proved in [22] that the growth of $\mathcal{C}(T)$ is exponentially

*Email: mniknam@uwaterloo.ca

bounded. More recently, it has been conjectured that the saturation of this bound should be an indicator of quantum chaos [23, 24], the rate being related with the classical Lyapunov exponent. This has been confirmed for one-body chaotic systems [25, 26] and for the Dicke model [27], but not yet for interacting many-body quantum systems.

Our echo experiment shows that the OTOC has a Gaussian decay in time, but an exponential behavior is revealed when the OTOC is studied as a function of the average of Hamming weights for the multi-spin correlations. The ability of our experiment to directly map these correlations is an essential ingredient for uncovering the flow of quantum information and the exponential decay of the OTOC.

Sample description

The sample studied is a polycrystalline solid at room temperature composed of an ensemble of triphenylphosphine molecules, as shown in Fig. 1a. Each molecule has a central ^{31}P nuclear spin coupled to fifteen ^1H environment spins via the heteronuclear dipolar interaction

$$\mathcal{H}_{SE} = \sum_j^N \omega_j \sigma_z^{\text{cs}} \otimes \sigma_z^j, \quad (2)$$

where N is the number of environment spins and $\sigma_{x,y,z}^j$ represent Pauli matrices for the j^{th} spin. The dipolar Hamiltonian is a second rank spherical tensor, where $\omega_j \propto (3 \cos^2 \theta_j - 1)/r_j^3$ has radial and angular dependence on the vector \vec{r}_j connecting the central spin to the j^{th} spin in the environment. In this coupling constant, θ_j is the angle between \vec{r}_j and the static field of the NMR magnet. Therefore, an environment spin located near the cone defined by the magic angle θ_M , with $3 \cos^2 \theta_M - 1 = 0$, does not interact with the central spin. The orientation of the sample molecule illustrated in Fig. 1a is such that two of the environment spins lie on the magic-angle cone and consequently, do not interact with the central spin. They belong to the ‘‘non-connected’’ group, while environment spins coupled to the central spin are part of the ‘‘connected’’ group, as sketched in Fig. 1b. The size of the connected group grows in time (see Methods).

The central spin is initially in the state $\rho^{\text{cs}}(0) = [\mathbb{1} + \epsilon \sigma_x]/2$, where ϵ is the strength of the nuclear spin polarization and is of the order of 10^{-6} at room temperature. In what follows, we drop the identity operator to simplify the notation. The N spins in the environment are in the maximally mixed state $\rho^{\text{env}}(0) = (\mathbb{1}/2)^{\otimes N}$, with no correlations and no information content. Thus, the initial state of the composite system is uncorrelated

$$\rho(0) = \rho^{\text{cs}}(0) \otimes \rho^{\text{env}}(0). \quad (3)$$

Mapping the multi-spin correlations

We design an echo experiment, which we call multi-spin correlation detection (MCD), to detect the correlation buildup between the central spin and the environment spins. The stages of the MCD experiment are sketched in Fig. 2a (see Methods for NMR pulse sequence). During the evolution time T , the environment self-interaction is averaged to zero

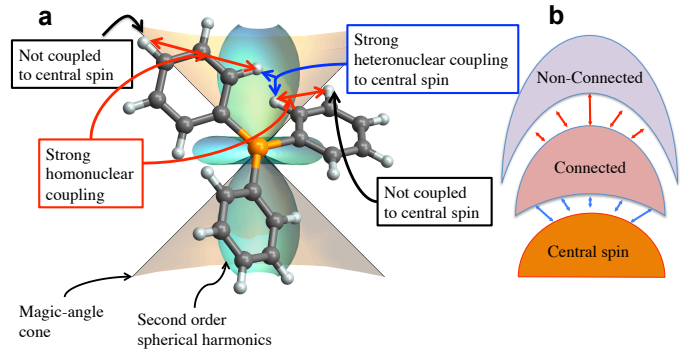


FIG. 1: **Sample structure matching the central spin model.** The Triphenylphosphine molecule shown in panel a has a ^{31}P nucleus at the central spin position and fifteen ^1H nuclei as the environment spins. Due to the angular dependence of the dipolar interaction, environment spins located near the two magic-angle cones (shaded area) are very weakly coupled to the central spin. The connected and non-connected groups are sketched in b.

using the MREV-8 pulse sequence [16], while the remaining system-environment interaction correlates the two. The dynamics is described by the unitary propagator $U_{SE}(T) = e^{-i\tilde{\mathcal{H}}_{SE}T}$, where tilde represents the Hamiltonian in the toggling frame of the MREV-8 pulse [15]. This experiment builds upon multiple quantum NMR techniques developed to characterize coherence orders in solid state samples [28–37].

After the evolution with the system-environment Hamiltonian, the resulting density matrix $\rho(T) = U_{SE}(T)\rho(0)U_{SE}^\dagger(T)$ may be described using the number of coupled spins and the weight of each cluster c_n :

$$\begin{aligned} \rho(T) = & c_0(T) \sigma_x^{\text{cs}} \otimes \mathbb{1}^N \\ & + c_1(T) \sum_i^N \sigma_y^{\text{cs}} \otimes \sigma_z^i \otimes \mathbb{1}^{N-1} \\ & + c_2(T) \sum_{i \neq j}^N \sigma_x^{\text{cs}} \otimes \sigma_z^i \otimes \sigma_z^j \otimes \mathbb{1}^{N-2} \\ & + \dots \end{aligned} \quad (4)$$

The density matrix terms describing various cluster size, correspond to different correlation orders in the x quantization axis where the ladder operators are defined as $\sigma_{x\pm}^i = \sigma_y^i \pm i\sigma_z^i$ (see Methods). In that frame the correlation order is determined by the number of σ_{x+} operators minus σ_{x-} operators, or the Hamming weight of each term. The result of such transformation for the density matrix in equation (4) can be

arranged as:

$$\begin{aligned}
&= C_0(T) \sum_{i \neq j}^N \sigma_x^{cs} \otimes [\mathbb{1}^N - (\sigma_{x+}^i \otimes \sigma_{x-}^j \otimes \mathbb{1}^{N-2}) + \dots] \\
&+ C_1(T) \sum_i^N \sigma_y^{cs} \otimes [(\sigma_{x+}^i \otimes \mathbb{1}^{N-1}) - (\sigma_{x-}^i \otimes \mathbb{1}^{N-1}) \\
&+ \dots] \\
&+ C_2(T) \sum_{i \neq j}^N \sigma_x^{cs} \otimes [(\sigma_{x+}^i \otimes \sigma_{x+}^j \otimes \mathbb{1}^{N-2}) + (\sigma_{x-}^i \otimes \sigma_{x-}^j \otimes \mathbb{1}^{N-2}) \\
&+ \dots] \\
&+ \dots, \tag{5}
\end{aligned}$$

where C_n indicates the weight of terms with the same correlation order. Using this representation corresponds to expressing the density matrix of the system-environment in the basis spanned by the multi-spin correlation terms of order n , $\rho(T) = \sum_{n=0}^N C_n(T) \rho_n$. The order n is encoded in a phase factor by performing a collective rotation of the environment spins by an angle ϕ along the x -axis, $R_x(\phi) = \exp\left(i \frac{\phi}{2} \sum_j^{\text{env}} \mathbb{1}^{cs} \otimes \sigma_x^j\right)$ which results in

$$\rho_\phi(T) = R_x(\phi) \rho(T) R_x^\dagger(\phi) = \sum_{n=0}^N e^{in\phi} C_n(T) \rho_n.$$

After the rotation, the system-environment Hamiltonian is reversed to create an observable echo signal at time $2T$, $S_\phi(2T) = \text{Tr}[\rho_\phi(2T)\rho(0)]$, where

$$\rho_\phi(2T) = U_{SE}^\dagger(T) R_x(\phi) U_{SE}(T) \rho(0) U_{SE}^\dagger(T) R_x^\dagger(\phi) U_{SE}(T).$$

The Fourier transform of $S_\phi(2T)$ gives the correlation amplitudes, $|C_n(T)|^2$, as shown in Fig. 2b. A map of the correlation production is obtained by following the changes in the correlation amplitudes as a function of T , depicted in Fig. 2c. If we consider the spread of correlations occurring in consecutive time steps, correlation order n contributes to orders $n+1$ and $n-1$ in the next time step.

At time T , the amplitudes $|C_n(T)|^2$ provide a snapshot of the system-environment correlations. The distribution of the correlation orders weighted by $|C_n(T)|^2$ can be approximated with a Gaussian shape. We use the second moment of the correlation amplitudes $\sum_n^N |C_n(T)|^2 n^2$, that is the width of this distribution, as a measure of the extent of correlations between the central spin and the environment. This quantity is referred to as ‘‘average number of correlated spins’’ or ‘‘average Hamming weight’’ of the spin system, and it is related to the QFI.

In its most general form, the QFI is defined as [6], $\mathcal{F}_Q(\rho_x) := 4\partial_x^2 D_B^2(\rho_{x_0}, \rho_x)|_{x=x_0}$, where the Bures distance $D_B^2(\rho, \sigma) := 2[1 - f(\rho, \sigma)]$ measures the distance between two close density matrices ρ and σ , with $f(\rho, \sigma) = \text{Tr}[\sqrt{\sqrt{\rho}\sigma\sqrt{\rho}}]$ being the fidelity. In the MCD experiment, the second derivative of our observable echo signal $S_\phi(2T)$ in equation (??), with the rotation angle ϕ replacing the real

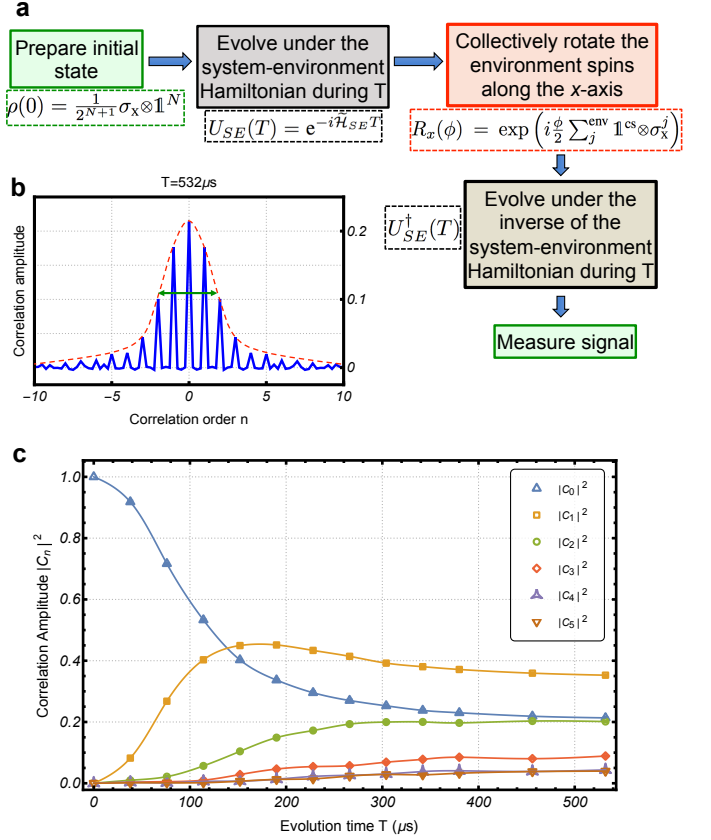


FIG. 2: **The multi-spin correlation detection (MCD) experiment.** Various stages of the MCD experiment are sketched in the panel a. The plot for the correlation amplitudes in panel b displays the distribution of the system-environment correlations at a chosen time T . The time evolution of the correlation amplitudes $|C_n(T)|^2$ in panel c indicates the spread of correlations between the system and environment. The error bars, corresponding to the inverse of the signal to noise ratio are very small and not visible in panel c.

parameter x , is related to the second moment of the correlation spectra,

$$\begin{aligned}
-\left. \frac{\partial^2 S_\phi(2T)}{\partial \phi^2} \right|_{\phi=0} &= -\left. \frac{\partial^2 \text{Tr}[\rho_\phi(2T)\rho(0)]}{\partial \phi^2} \right|_{\phi=0} \\
&= -\left. \frac{\partial^2 \text{Tr}[\rho_\phi(T)\rho(T)]}{\partial \phi^2} \right|_{\phi=0} \\
&= -2 \sum_{n=0}^N \left. \frac{\partial^2 e^{in\phi} |C_n(T)|^2 \rho_n^2}{\partial \phi^2} \right|_{\phi=0} \\
&= -2 \sum_{n=0}^N n^2 |C_n(T)|^2. \tag{6}
\end{aligned}$$

For a quantum system in the pure state, this quantity is equal to the QFI and for a many-body system with mixed states, Gärtner et. al. showed that it gives a lower bound on the QFI [19].

In Fig. 3, we show the evolution of the average Hamming weight. The curve indicates that as time passes, quantum in-

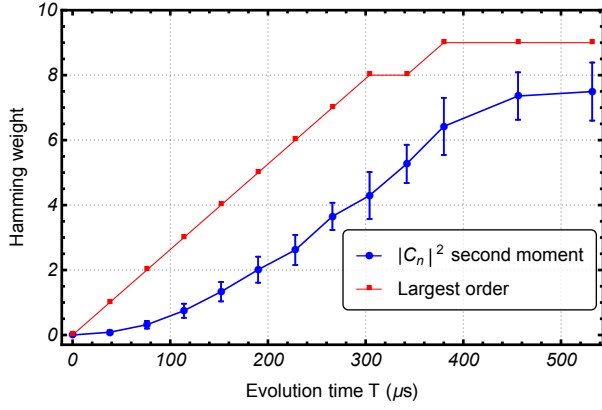


FIG. 3: **Flow of quantum Fisher information.** The second moment of the distribution of multi-spin correlations (Hamming weight) and the largest correkation order as a function of time. The second moment of the distribution is used to quantify the average size of correlations and the flow of quantum information. The information flow has a slow initial rate and becomes linear before saturation. The largest correlation order indicates the size of the fastest growing correlations in the spin ensemble.

formation is on average shared with a larger subset of environment spins or, equivalently, it flows outward from the system. The flow of quantum information is not linear throughout the evolution. It is initially slow, followed by a regime of linear increase before saturation. The point of saturation depends on the size of the connected group of environment spins (see Methods). The rate of change of QFI ($\partial\mathcal{F}_Q/\partial t$), has been proposed as a measure for quantum information flow [5]. Therefore, the slope of the average Hamming weight in Fig. 3 corresponds to the flow of quantum information.

Scrambling of information in the environment

The environment spins interact via the homonuclear dipolar Hamiltonian

$$\mathcal{H}_E = \mathbb{1}^{\text{cs}} \otimes \sum_{j < k}^N \Omega_{jk} \left[\sigma_z^j \sigma_z^k - \frac{1}{4} (\sigma_+^j \sigma_-^k + \sigma_-^j \sigma_+^k) \right], \quad (7)$$

where $\Omega_{jk} \propto (3 \cos^2 \theta_{jk} - 1)/r_{jk}^3$ is the coupling strength between the environment spins j and k , and the operators in parenthesis represent the flip-flop term that swaps the states of pairs of environment spins. The eigenvalues of this Hamiltonian satisfy level statistics given by random matrix theory (see Methods), as in quantum systems with chaotic classical counterparts. Consequently, the scrambling of information within the environment is expected to take place very fast.

To analyze the sensitivity of quantum information to scrambling in the environment, we used the echo experiment outlined in Fig. 4a. In this experiment, the evolution interval T , where only the coupling between the system and the environment is effective, is followed by a scrambling window of length τ , where only the environment spins interact and the propagator is $U_E(\tau) = e^{-i\mathcal{H}_E\tau}$. The observable echo signal amplitude at $2T + \tau$ is $S(2T + \tau) = \text{Tr}[\rho(2T + \tau)\rho(0)]$, where

$$\rho(2T + \tau) = U_{SE}^\dagger(T) U_E(\tau) U_{SE}(T) \rho(0) U_{SE}^\dagger(T) U_E^\dagger(\tau) U_{SE}(T).$$

The signal $S(2T + \tau)$ for a fixed scrambling window τ can be written as the OTOC function

$$F_\tau(T) = \text{Tr}[W_\tau^\dagger(T) \rho(0) W_\tau(T) \rho(0)] \quad (8)$$

where we defined the initial density matrix $\rho(0)$ as the $V(0)$ operator in equation (1) and

$$W_\tau(T) = U_{SE}^\dagger(T) U_E^\dagger(\tau) U_{SE}(T). \quad (9)$$

The operator $V(0) = \rho(0)$ commutes with $W_\tau(0) = U_E(\tau)$. The information that is shared with the environment in the course of time T can get scrambled during τ . The length of the scrambling window τ characterizes the strength of the environment perturbation. The level of sensitivity of quantum information to perturbations in the environment is reflected by the non-commutivity between $V(0)$ and $W_\tau(T)$ for $T > 0$.

In Fig. 4b the results for the OTOC experiment are presented for various evolution and perturbation times. When $\tau = 0$, the state of the central spin is completely refocused (revived) and $F_{\tau=0}(T) = 1$ for any T . This happens because during the evolution time, the information initially encoded in the central spin is not lost, but is simply stored in the form of multi-spin correlations between the system and the environment spins from the connected group. By reversing the evolution, the information can be recovered by the system.

The refocusing degrades and the echo amplitude decays as τ increases. During the scrambling window, the flip-flop term of \mathcal{H}_E exchanges the states of pairs of coupled spins in the environment. As a result, the subsequent evolution under the inverse of the system-environment Hamiltonian can only partially revive the initial state. This situation is aggravated by the

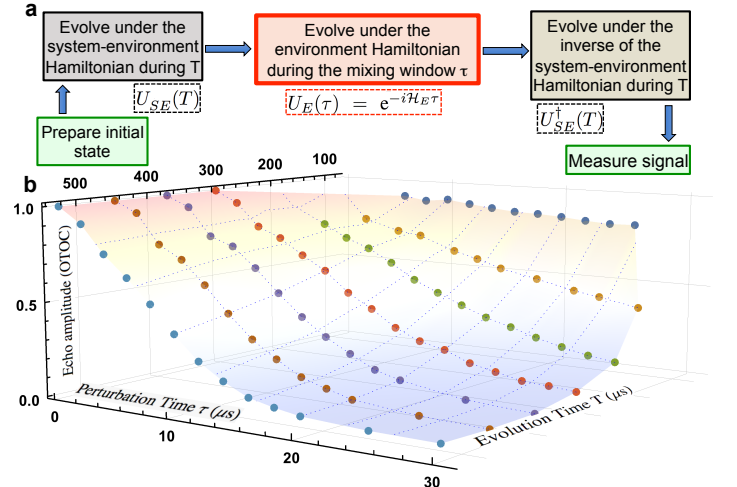


FIG. 4: **The OTOC function measures the sensitivity of quantum information to environment perturbations.** Sketch of the steps involved in the OTOC experiment is depicted in a. The decay of the echo amplitude as a function of the evolution time T is shown in b. For small perturbations (short τ), the central spin for most molecules gets refocused and the OTOC is nearly independent of T , while for large perturbations, the OTOC decays significantly with T .

existence of the non-connected group of environment spins, which do not develop correlations with the central spin during T , but may have their states swapped with those from other environment spins during the scrambling window. Information that is shared with the non-connected group cannot be recovered, which ultimately leads to the loss of quantum information in the environment. It is in general expected that quantum information is more sensitive to perturbations if more information is shared with the environment.

Inspired by the not always linear flow of quantum information in Fig. 3, we now compare the behavior of the OTOC as a function of the evolution time T in Fig. 5a with the OTOC as function of the average Hamming weight in Fig. 5b.

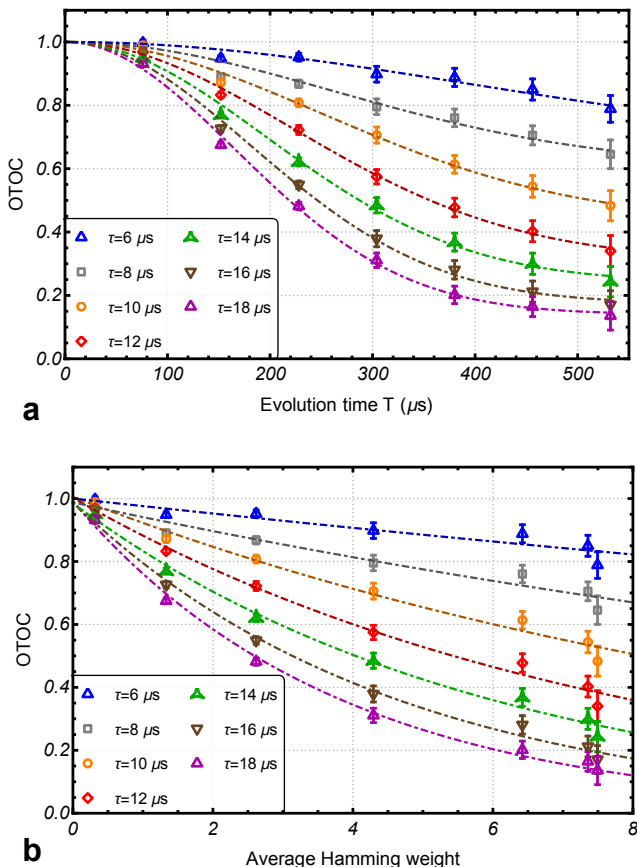


FIG. 5: The OTOC decays exponentially with the extent of information in the environment. Panel **a** depicts the OTOC as a function of the evolution time T and **b** as a function of the average Hamming weight. Each curve in the panels corresponds to a fixed value of the scrambling window τ (perturbation strength). The data are normalized with respect to the $\tau = 0$ data set. The dashed lines in **a** and **b** are Gaussian and exponential fits, respectively. The exponential behavior is uncovered by analyzing the OTOC decay as a function of the average Hamming weight. Because of the environment's finite size and the memory effects, the late decay data is better described by a Gaussian function. Error bars in panel **a** and **b** indicate the inverse of signal to noise ratio.

As seen in Fig. 5a, the OTOC decay in time is well described by a Gaussian function. This is expected since the

evolution in the environment during the scrambling window is governed by an ensemble of U_E unitaries. This is similar to what one finds in free induction decay experiments for environment spins, where the signal decay is also Gaussian. There are also several examples of solid systems with coupling constants from a normal distribution, where the spin signal is well approximated by a Gaussian function [38, 39].

In Fig. 5b, we shift the perspective and analyze the OTOC as a function of the average Hamming weight. By doing this, we remove the effects of the system-environment unitary evolution. This is motivated by the fact that the amplitude of the echo signal is inversely proportional to the probability of spin pair flip-flops and the number of correlated spins in the environment. The resulting behavior of the OTOC is an exponential decay corroborated by the exponential fits in Fig. 5b. The exponential decay indicates that at each time step the average Hamming weight is the defining factor for the decay rate of the echo amplitude, regardless of what happened to the system at earlier times. This confirms that the average Hamming weight, or the second moment of the correlation spectrum, is an appropriate measure for the quantum information shared with the environment.

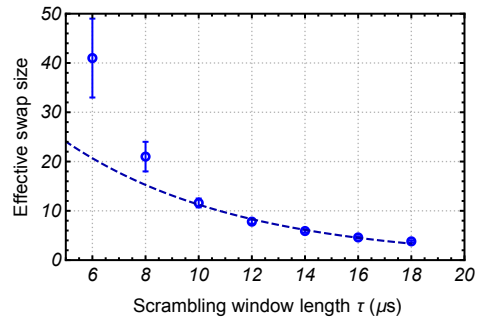


FIG. 6: Effective swap size of the OTOC, decreases exponentially with τ , as indicated with the exponential fit (dashed line). The error bars correspond to the errors for the exponential fits in Fig. 5b. Similar dynamics is observed for swapping coins in a classical coin game (see Methods).

Figure 6 indicates the effective swap size constants, evaluated from the exponential fits in Fig. 5b. Similar to the concept of decay characteristic time, the effective swap size indicates the average system-environment correlation size necessary for a given perturbation to be effective in decreasing the echo signal amplitude by a factor of $1/e$ in Fig. 5b. For the small scrambling windows $\tau = 6, 8 \mu\text{s}$, there is no such size, as the perturbation is too small and leaves the environment unchanged for most orientations of the environment spins. This results in the unreasonably large values for the effective swap size in Fig. 6. With the increase of the perturbation strength, smaller correlations can be scrambled efficiently. Consequently, the effective swap sizes decay exponentially with τ . This is in agreement with the decay rates obtained in a classical coin game designed to simulate the scrambling dynamics (see Methods). These results indicate the effectiveness of the environment perturbations in scrambling quantum information which can be used to prevent quantum informa-

tion backflow from the environment to the system.

In conclusion, we designed a multi-spin correlation detection experiment to directly quantify the growth of correlations between the central spin and its environment. The second moment of the distribution of correlations provides a measure of the amount of quantum information shared with the environment and puts a bound on the flow of QFI in the system.

We also used the OTOC to quantify the sensitivity of quantum information to perturbations in the environment. The OTOC shows a Gaussian behavior in time, but decays exponentially with respect to the amount of information shared with the environment. Our experiment provides a new way to analyze non-equilibrium quantum dynamics, where instead of approaching the evolution as a unitary process, quantities of interest are studied as a function of the flow of quantum information.

Although the separation of the system-environment evolution and the scrambling process in the environment enables us to study the effects of each Hamiltonian with clarity, this is not a necessary step for the detection of information flow. In fact, the correlation detection technique developed in this work can be used in general for any qubit system as long as a global control of the environment is possible.

Acknowledgments

The research results communicated here would not be possible without the significant contributions of the Canada First Research Excellence Fund, Canada Excellence Research Chairs program, Canada Foundation for Innovation, the Ontario Ministry of Research & Innovation, Industry Canada and Mike & Ophelia Lazaridis. Their support is gratefully acknowledged. L.F.S. was supported by the American NSF grant No. DMR-1603418.

-
- [1] Bennett, C. H. & DiVincenzo, D. P. Quantum information and computation. *Nature* **404**, 247–255 (2000).
- [2] Myatt, C. J., King, B. E., Turchette, Q. A., Sackett, C. A., Kielpinski, D., Itano, W. M., Monroe, C. & Wineland, D. J. Decoherence of quantum superpositions through coupling to engineered reservoirs. *Nature* **403**, 269–273 (2000).
- [3] Breuer, H.-P., Laine, E.-M. & Piilo, J. Measure for the Degree of Non-Markovian Behavior of Quantum Processes in Open Systems. *Phys. Rev. Lett.* **103**, 210401 (2009).
- [4] Bylicka, B., Johansson, M. & Acín, A. Constructive Method for Detecting the Information Backflow of Non-Markovian Dynamics. *Phys. Rev. Lett.* **118**, 120501 (2017).
- [5] Lu, X.-M., Wang, X. & Sun, C. P. Quantum Fisher information flow and non-Markovian processes of open systems. *Phys. Rev. A* **82**, 042103 (2010).
- [6] Yadin, B. & Vedral, V. General framework for quantum macroscopicity in terms of coherence. *Phys. Rev. A* **93**, 022122 (2016).
- [7] Braunstein, S. L. & Caves, C. M. Statistical distance and the geometry of quantum states. *Phys. Rev. Lett.* **72**, 3439–3443 (1994).
- [8] Khaetskii, A. V., Loss, D. & Glazman, L. Electron Spin Decoherence in Quantum Dots due to Interaction with Nuclei. *Phys. Rev. Lett.* **88**, 186802 (2002).
- [9] Cucchietti, F. M., Paz, J. P. & Zurek, W. H. Decoherence from spin environments. *Phys. Rev. A* **72**, 052113 (2005).
- [10] Yang, W. & Liu, R.-B. Quantum many-body theory of qubit decoherence in a finite-size spin bath. II. Ensemble dynamics. *Phys. Rev. B* **79**, 115320 (2009).
- [11] de Gennes, P.-G. Sur la relaxation nucléaire dans les cristaux ioniques. *Journal of Physics and Chemistry of Solids* **7**, 345–350 (1958).
- [12] Anderson, P. W. Spectral Diffusion, Phonons, and Paramagnetic Spin-Lattice Relaxation. *Phys. Rev.* **114**, 1002–1005 (1959).
- [13] Gaudin, M. Diagonalisation d’une classe d’Hamiltoniens de spin. *J. Phys. France* **37**, 1087–1098 (1976).
- [14] Prokof’ev, N. V. & Stamp, P. C. E. Theory of the spin bath. *Reports on Progress in Physics* **63**, 669 (2000).
- [15] Haeberlen, U. *High Resolution NMR in Solids: Selective Averaging* (Academic Press, New York, 1976).
- [16] Rhim, W., Elleman, D. D. & Vaughan, R. W. Enhanced resolution for solid state NMR. *J. Chem. Phys.* **58**, 1772–1773 (1973).
- [17] Gerstein, B. C. & Dybowski, C. R. *Transient techniques in NMR of solids* (Academic Press, Inc., 1985).
- [18] Gärtner, M., Bohnet, J. G., Safavi-Naini, A., Wall, M. L., Bollinger, J. J. & Rey, A. M. Measuring out-of-time-order correlations and multiple quantum spectra in a trapped-ion quantum magnet. *Nat. Phys.* **13**, 781–786 (2017).
- [19] Gärtner, M., Hauke, P. & Rey, A. M. Relating Out-of-Time-Order Correlations to Entanglement via Multiple-Quantum Coherences. *Phys. Rev. Lett.* **120**, 040402 (2018).
- [20] Li, J., Fan, R., Wang, H., Ye, B., Zeng, B., Zhai, H., Peng, X., & Du, J. Measuring Out-of-Time-Order Correlators on a Nuclear Magnetic Resonance Quantum Simulator. *Phys. Rev. X* **7**, 031011 (2017).
- [21] Wei, K. X., Ramanathan, C. & Cappellaro, P. Exploring Localization in Nuclear Spin Chains. *Phys. Rev. Lett.* **120**, 070501 (2018).
- [22] Lieb, E. H. & Robinson, D. W. The Finite Group Velocity of Quantum Spin Systems. *Comm. Math. Phys.* **28**, 251 (1972).
- [23] Kitaev, A. Y. A simple model of quantum holography. <http://online.kitp.ucsb.edu/online/entangled15/kitaev/> & <http://online.kitp.ucsb.edu/online/entangled15/kitaev2/>. note.
- [24] Maldacena, J., Shenker, S. H. & Stanford, D. A bound on chaos. *J. High Energ. Phys.* **2016**, 106 (2016).
- [25] Rozenbaum, E. B., Ganeshan, S. & Galitski, V. Lyapunov Exponent and Out-of-Time-Ordered Correlator’s Growth Rate in a Chaotic System. *Phys. Rev. Lett.* **118**, 086801 (2017).
- [26] Rozenbaum, E. B., Ganeshan, S. & Galitski, V. Universal Level Statistics of the Out-of-Time-Ordered Operator. arXiv: 1801.10591.
- [27] Chávez-Carlos, J., López-del-Carpio, B., Bastarrachea-Magnani, M. A., Stránský, P., Lerma-Hernández, S., Santos, L. F., Jorge Hirsch, J. G. Quantum and Classical Lyapunov Exponents in Atom-Field Interaction Systems. arXiv: 1807.10292.
- [28] Baum, J., Munowitz, M., Garroway, A. N. & Pines, A. Multiple-quantum dynamics in solid state NMR. *J. Chem. Phys.* **83**, 2015–2025 (1985).
- [29] Munowitz, M., Pines, A. & Mehring, M. Multiple-quantum dynamics in NMR: A directed walk through Liouville space. *J.*

- Chem. Phys.* **86**, 3172–3182 (1987).
- [30] Munowitz, M. *Coherence and NMR* (John Wiley & Sons, Inc., 1988).
- [31] Lacelle, S., Hwang, S.-J. & Gerstein, B. C. Multiple quantum nuclear magnetic resonance of solids: A cautionary note for data analysis and interpretation. *J. Chem. Phys.* **99**, 8407–8413 (1993).
- [32] Ramanathan, C., Cho, H., Cappellaro, P., Boutis, G. S. & Cory, D. G. Encoding multiple quantum coherences in non-commuting bases. *Chem. Phys. Lett.* **369**, 311–317 (2003).
- [33] Krojanski, H. G. & Suter, D. Scaling of Decoherence in Wide NMR Quantum Registers. *Phys. Rev. Lett.* **93**, 090501 (2004).
- [34] Cho, H., Ladd, T. D., Baugh, J., Cory, D. G. & Ramanathan, C. Multispin dynamics of the solid-state NMR free induction decay. *Phys. Rev. B* **72**, 054427 (2005).
- [35] van Beek, J. D., Carravetta, M., Antonioli, G. C. & Levitt, M. H. Spherical tensor analysis of nuclear magnetic resonance signals. *J. Chem. Phys.* **122**, 244510 (2005).
- [36] Lovrić, M., Krojanski, H. G. & Suter, D. Decoherence in large quantum registers under variable interaction with the environment. *Phys. Rev. A* **75**, 042305 (2007).
- [37] Sánchez, C. M., Levstein, P. R., Buljubasich, L., Pastawski, H. M. & Chattah, A. K. Quantum dynamics of excitations and decoherence in many-spin systems detected with Loschmidt echoes: its relation to their spreading through the Hilbert space. *Philosophical Transactions of the Royal Society A: Mathematical, Physical and Engineering Sciences* **374** (2016).
- [38] Abragam, A. *The Principles of Nuclear Magnetism* (Oxford University Press, 1961).
- [39] Cho, H., Cappellaro, P., Cory, D. G. & Ramanathan, C. Decay of highly correlated spin states in a dipolar-coupled solid: NMR study of CaF_2 . *Phys. Rev. B* **74**, 224434 (2006).
- [40] Guhr, T., Mueller-Gröeling, A. & Weidenmüller, H. A. Random Matrix Theories in Quantum Physics: Common Concepts. *Phys. Rep.* **299**, 189 (1998).

Methods

A. Sample

Triphenylphosphine is a common organophosphorous compound and was obtained from SIGMA-ALDRICH with 99% purity. To reduce the T_1 relaxation time of the protons we used Chromium(III) acetylacetonate as a relaxation agent. 1 mmol of the sample and 0.13 mmol of the relaxation agent were resolved in 300 ml of Chloroform-d and left for crystallization over night. The resulting powder was compressed into a NMR-sphere sample tube which was flame sealed to best preserve the contents. Using the relaxation agent resulted in reduction of the proton T_1 relaxation time from $630 \pm 30\text{s}$ to $2.5 \pm 0.2\text{s}$.

B. Spin groups in the environment

The dipolar interaction strength depends on the relative orientation of spins with respect to the static field of the NMR magnet. The multi-spin correlation development and the information scrambling in the environment, both depend on the strength of the dipolar interactions which is determined by the structure and the orientation of the sample molecules. The idea of distinguishing between a group of environment spins that is connected with the central spin from a group that is not connected can be explored by considering the number of spins in the environment with strong couplings to the central spin. These spins are more likely to become correlated during the evolution time. Figure 7 plots the average number of environment spins correlated to the central spin, with a probability larger than $\frac{1}{2}$ in the MCD experiment. Heteronuclear dipolar coupling constants are evaluated for 2000 randomly orientated Triphenylphosphine molecules. For the longest evolution time in the MCD experiment, $T = 532 \mu\text{s}$, 11 environment spins are found to be more likely to correlate with the central spin, on average.

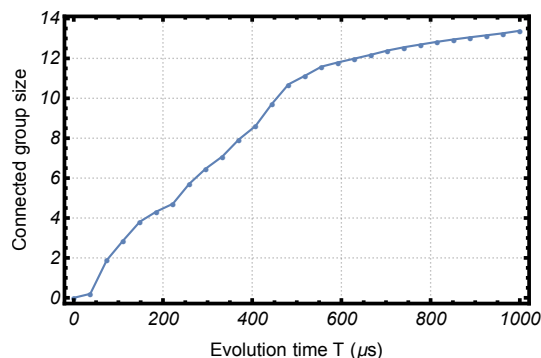


FIG. 7: A simulation of 2000 random orientations of the Triphenylphosphine molecule is used to estimate the size of the connected spin group for various evolution times in the MCD experiment.

C. NMR experiments

The MCD experiment captures a snapshot of the multi-spin correlations between the central spin and the environment at a specific evolution time. This experiment is designed to initiate the growth of correlations from the central spin and also to use the central spin itself as a probe for detection of the multi-spin correlated states. Figure 8a shows a two channel NMR pulse program used for simultaneous control of the central spin (^{31}P) and the environment spins (^1H) in the MCD experiment. The Cross Polarization (CP) pulse sequence is used to remove environment correlations and to increase the signal to noise ratio of the experiment by enhancing the initial polarization of the central spin. Evolution under the heteronuclear dipolar interaction for time T results in the growth of system-environment correlations, while the homonuclear dipolar interaction in the environment is averaged out with the MREV-8 pulse sequence. Application of a collective rotation ϕ_x on the environment spins encodes their correlation order as a phase factor. The π pulse on the central spin, inverts the heteronuclear dipolar Hamiltonian to make this an echo experiment with the refocused signal appearance at time $2T$.

Figure 8b sketches the pulse sequence used for measuring the OTOC decay. In this experiment, the collective rotation of the environment spins is removed and a scrambling window is introduced. During this window, the environment spins evolve under the homonuclear dipolar interaction while the central spin is decoupled from them. The echo signal at the end of this experiment gives the amplitude of the multi-spin correlated terms that were not affected by the homonuclear dipolar interaction during the scrambling window.

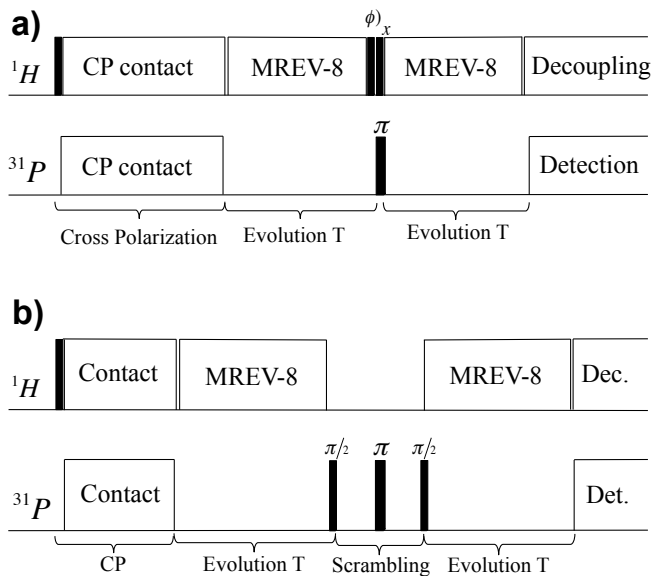


FIG. 8: NMR pulse sequence for the Multi-spin Correlation Detection (MCD) experiment is shown in panel **a**. Panel **b** displays the pulse sequence for OTOC measurement with quantum information scrambling implementation in the environment.

D. Correlation orders vs number of correlated spins

The ladder operators in the x quantization axis are defined as $\sigma_{x\pm}^i = \sigma_y^i \pm i\sigma_z^i$ and as a result $\sigma_z^i = \frac{\sigma_{x+}^i - \sigma_{x-}^i}{2i}$. Each σ_z in equation (4) corresponds to correlation orders of ± 1 .

In the case of two environment spins correlated to the central spin, $\sigma_z \otimes \sigma_z$, the correlation terms produced in the MCD experiment are

$$-\frac{1}{4}(\sigma_{x+} \otimes \sigma_{x+}), \frac{1}{4}(\sigma_{x+} \otimes \sigma_{x-}), \frac{1}{4}(\sigma_{x-} \otimes \sigma_{x+}), -\frac{1}{4}(\sigma_{x-} \otimes \sigma_{x-}).$$

The correlation spectrum for $\sigma_z \otimes \sigma_z$ consists therefore of three peaks positioned at $-2, 0$ and 2 with amplitudes $\frac{1}{4}, \frac{1}{2}$ and $\frac{1}{4}$ respectively.

It is easy to see that having odd(even) number of correlated spins in the environment, results in a spectrum of peaks in odd(even) positions with amplitudes of the binomial distribution. Therefore, the largest observed correlation order always corresponds to the number of correlated environment spins, albeit with an amplitude that scales with $\frac{1}{2^n}$. Consequently, the width of the correlation order spectrum is more suitable as a measure for the extent of correlations than the largest observed order.

E. Classical coin game

We have designed a classical game to make a parallel with the swap dynamics of the environment spins. Consider an array of N coins initially set to heads. We randomly flip k of these coins, where each coin may be flipped only once, to represent spins in the connected group at time T . If no swap actions occurs, flipping the same random k coins for a second time results in the complete return to the initial state. This is equivalent to a perfect echo of the spin signal at time $2T$. When we add random swap actions between the two flipping stages, the final state of the coin array may be different from its initial state. The distant between the initial and final state of the coin array depends of the number of swaps performed and the probability of having a swap between a flipped and an un-flipped coin. The probability of having this sort of “successful swap” (ssw) is given by

$$P_{ssw} = 2 \frac{kN - k^2}{N^2 - N}. \quad (10)$$

For this simple example we are ignoring the cases where the same two coins swap more than once and we assume that after each swap the probability of having a successful swap remains unchanged. Therefore the probability of success for m random coin swaps is considered to be m times the probability of success for one coin swap. Consequently, the overlap amplitude between initial state and the final state of the coin chain after two rounds of flipping with a round of spin swap

in the middle is

$$\begin{aligned} A_{OL}(m, k, N) &:= \left(1 - \frac{2m}{N} P_{ssw}\right)^2 \\ &= \left(1 - \frac{4m}{N} \frac{kN - k^2}{N^2 - N}\right)^2. \end{aligned} \quad (11)$$

$A_{OL}(m, k, N)$ is plotted in Fig. 9 for an array of $N = 15$ coins, which is the number of environment spins, while k is set according to the average Hamming weights for various evolution time steps T in the MCD experiment, and m is varied from 1 to 15. We have fitted the data in Fig.9 with decaying

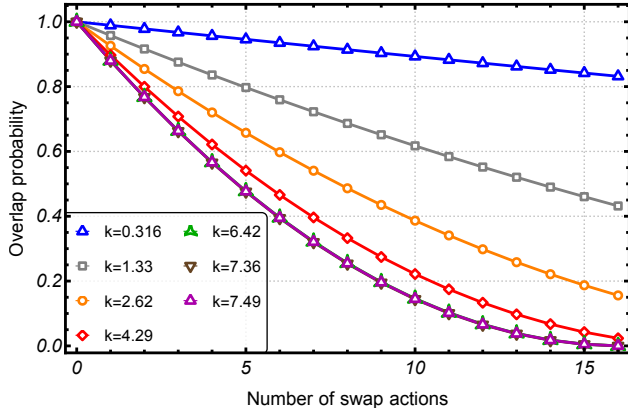


FIG. 9: The classical coin game is similar to the scrambling of quantum information in the spin environment. The overlap between the initial and final state of the coin array decays with the number of performed coin swaps.

exponential functions to evaluate the effective swap size for them. The result is plotted in Fig. 10. Similar to the OTOC experimental results, the effective swap size shows an exponentially decaying behavior, when the number of swap actions is less than the size of the system.

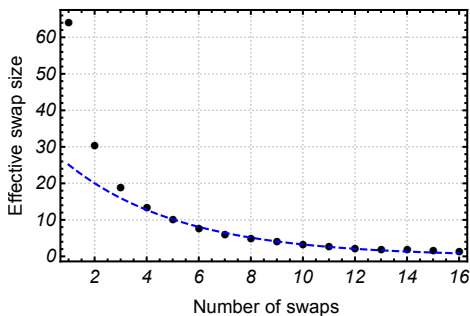


FIG. 10: The effective swap size for $m > 4$ shows an exponentially decaying behavior, similar to the experimental results for the OTOC. The dashed line indicates an exponential fit for this part of the data. For $m < 4$ the effective swap size is larger than the size of the coin array, which means that information scrambling cannot be performed effectively.

F. Chaotic environment

The quantum environment described by equation (3) is chaotic and therefore a fast scrambler of information. Quantum chaos refers to properties of the spectrum that indicate whether the classical counterpart of the quantum system is chaotic. One of the main signatures of chaos is the strong repulsion of the eigenvalues [40]. The energy levels of quantum systems that are classically chaotic are correlated and prohibited from crossing. This is detected, for example, with the distribution $P(s)$ of the unfolded spacings s between neighboring levels. In the case of real and symmetric Hamiltonian matrices, as in our case, the level spacing distribution follows closely the Wigner surmise,

$$P(s) = \frac{\pi s}{2} \exp\left(-\frac{\pi s^2}{4}\right). \quad (12)$$

We verified that $P(s)$ is indeed coincides with this equation for a single realization of the dipolar interactions.